Solution Structure of a Duplex DNA with an Abasic Site in a dA Tract†

Ke Yu Wang,‡,§ Sharon A. Parker,‡ Igor Goljer,|| and Philip H. Bolton*

Chemistry Department, Wesleyan University, Middletown, Connecticut 06459

Received June 18, 1997; Revised Manuscript Received July 31, 1997⊗

ABSTRACT: The presence of dA tracts in DNA can lead to stable curvature of the DNA, and this curvature can be important in gene regulation, DNA packaging, and other processes. Since damage to DNA may eliminate this stable curvature, the solution state structure of the duplex of d(CGCAAAAATGCG) paired with d(CGCATTDTTCCG), with D indicating an abasic site, has been determined. The undamaged DNA bends into the major groove both in solution and in the crystal state. The presence of the abasic site in the dA tract region induces changes in the DNA structure up to four base pairs away from the damaged site. The structure of the DNA is dependent on whether the abasic site is in the α or *β* hemiacetal form. These consequences are quite different from the more localized effects that have been observed for "normal" DNAs containing abasic sites. Thus, there appears to be a strong sequence dependence of the structural effects of abasic sites just as there is for undamaged DNA. Furthermore, these results indicate that the presence of an abasic site can alter DNA bending and hence is likely to have significant long range effects on gene regulation and other properties that are dependent on the stable curvature of DNA.

DNA damage can occur via a variety of routes, including oxidative stress, the action of chemical agents, and radiative processes (*1*−*8*). Base damage such as the spontaneous deamination of cytosine to uracil, the oxidation of thymine to thymine glycol, or the oxidation of guanine can be repaired via abasic site intermediates as can base methylation. The first step in base excision repair of DNA containing damaged bases *in vivo* is typically the hydrolytic cleavage of the C−N bond between the sugar and the damaged or unusual base, to generate an aldehydic abasic site which is sometimes referred to as an apurinic/apyrimidinic or AP site.

The abasic site is an equilibrium mixture of α- (**I**) and *β*-hemiacetals (**II**) which are 2-deoxy-D-*erythro*-pentofuranoses, of aldehyde (**III**), and of hydrated aldehyde (**IV**), as depicted below (*9*−*13*). The 3′ cleavage of the abasic site catalyzed by AP lyases or the enzyme formamidopyrimidine-DNA glycosylase, (Fpg) is via a syn *β*-elimination reaction (*10*, *14*), and the 5′ cleavage is via a *δ* elimination when catalyzed by Fpg (*14*).

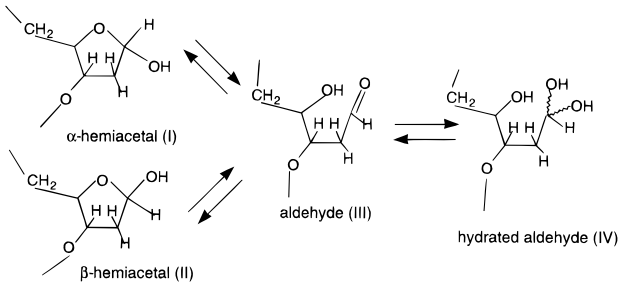

In many cells, the predominant pathway to the presence of aldehydic abasic sites is the spontaneous deamination of cytosine to uracil (*2*, *6*, *7*, *15*, *16*). The enzyme *N*-uracil glycoslyase excises uracil to form an aldehydic abasic site. For a typical *Escherichia coli*, there are about 40−400 such events per cell division and in a typical mammalian cell 4000−40000 uracil formed per cell division (*2*, *6*, *7*, *15*−*18*). Misincorporation of dUTP leads to over 10000 incorporations of dU per replicative cycle for 10^{10} base pairs (*19*).

The number of abasic sites in a "typical" human cell is not known as both the rate of formation of such sites and the rate of repair are dependent on many factors. Ames and co-workers have estimated that there are more than 10000 damaged sites, of all types, per typical human cell at any given time (*20*). The presence of a direct relationship between DNA damage and cancer is known, but the number and types of damage to DNA which are required for transformation to occur are just now being determined (*2*, *6*, *21*−*27*). The damage of mitochondrial DNA can also have pronounced effects, and the repair processes of mitochondria are not well-understood (*23*).

During the past few years, there has been a growing appreciation of the diversity of DNA repair responses and their relation to the cell cycle and apoptosis (*28*−*32*). In

† This research was supported, in part, by Grant NP-750 from the American Cancer Society. The 400 MHz NMR spectrometer was purchased with support from the National Science Foundation (Grant BIR 93-03077). The 500 MHz spectrometer was purchased with support from the National Science Foundation (Grant BIR-95-12478) and from the Camille and Henry Dreyfus Foundation.

* To whom correspondence should be sent. Telephone: 860-685-2668. Fax: 860-685-2211. E-mail: pbolton@wesleyan.edu.

‡ Contributed equally to the structure determination.

§ Current address: Gilead Sciences, 353 Lakeside Dr. Foster City, CA 94404.

|| Current address: Varian Associates, 25 Hanover Rd. Florham Park, NJ 07932.

⊗ Abstract published in *Advance ACS Abstracts,* September 15, 1997.

S0006-2960(97)01464-5 CCC: $14.00

many mature cells, DNA repair is highly coupled with transcription and the DNA that is not being actively transcribed is not repaired (*3*, *24*, *27*, *33*). In at least some mature cells, damaged DNA sites accumulate, and hence, the structural and dynamical consequences of DNA damage, and the intermediates in DNA repair, may be more important in mature than in dividing cells. It is now known that DNA repair can be strand specific with only the transcribed strand being repaired (*23*, *24*, *26*, *27*). It is also known that DNA repair can be gene specific with only the active gene regions being repaired (*15*, *16*). In mature nerve cells, there is apparently little DNA repair occurring and damaged sites accumulate, and this may be related to the aging process (*5*, *34*−*37*). Thus, while many studies have focused on the effects of damaged DNA on replication, it is now recognized that damaged DNA can also have pronounced effects on transcription and chromosome integrity (*6*, *21*, *38*, *39*), cellular aging (*5*, *36*), reverse transcriptase (*40*), and topoisomerase (*41*).

There is a wide range of evidence showing that the effects of DNA damage can depend on sequence context (*2*, *11*, *24*, *27*, *40*, *42*−*45*). Sequences of DNA containing dA tracts can exhibit curvature that can be monitored by observing the retardation of the DNA on nondenaturing gels as well as by direct structural determination. This curvature of DNA is thought to be important both in the molecular recognition events and in gene regulation. The curvature of DNA can allow regions of DNA which are very distant in sequence to be brought close together. Base substitution in dA tracts can disrupt gene regulation (*46*−*48*) as well as the termination of plus strand DNA synthesis by the reverse transcriptase of HIV (*49*). Therefore, it was of interest to determine if the presence of an abasic site within a dA tract region has a pronounced effect on the structure of the DNA and whether the structural change is of sufficient magnitude to affect gene regulation and the long range structure of DNA.

The "curved" duplex context examined here is

d(C_1 G_2 C_3 A_4 A_5 A_6 A_7 A_8 T_9 $G_{10}C_{11}G_{12}$)

d($G_{24}C_{23}G_{22}T_{21}T_{20}T_{19}T_{18}T_{17}A_{16}C_{15}G_{14}C_{13}$)

This DNA was chosen since there is extensive literature available about the gel electrophoretic and other properties of the AAAAAT sequence (*45*, *50*−*53*) as well as a crystal structure (*54*, *55*). This DNA was found to cocrystallize in two forms referred to as "up" and "down". To begin this study, we first determined the solution structure of the undamaged DNA for comparison with the crystal structures (*56*). The refined solution state structure was found to be very similar to the up crystal structure. Both the crystallography, and NMR-based studies concluded that the bending of this DNA is about 20° into the major groove (*54*−*56*).

The solution structure of the "normal" DNA duplex d($C_1G_2C_3G_4A_5D_6A_7C_8G_9C_{10}C_{11}$)-d($G_{22}C_{21}G_{20}C_{19}T_{18}A_{17}$-$T_{16}G_{15}C_{14}G_{13}G_{12}$), with D indicating a deoxyribose aldehyde abasic site and numbering from 5′ to 3′, has been previously determined by the combined use of NMR and restrained molecular dynamics (*57*). The backbone of this duplex DNA is regular, and the duplex is right-handed and B form. Conformational changes relative to the parent, undamaged DNA due to the presence of the abasic site were found to only extend to the base pairs adjacent to the lesion site. Similarly, the differences between the α and β forms only extended to the base pairs adjacent to the damaged site. When the sugar of the abasic site is in the β configuration, the deoxyribose is within the helix, whereas when the sugar is in the α configuration, the deoxyribose is out of the helix. The base of residue A_{17} in the position opposite the abasic site is predominantly stacked in the helix in both cases. A water molecule can apparently form a hydrogen bond bridge between the β abasic site and the opposing A_{17} on the complementary strand.

The methods that we have developed to determine the structures of the curved DNA and the structure of the normal damaged DNA have been combined to determine the structures of the α and β forms of the curved DNA containing an abasic site in the middle of a run of dT residues. Unlike the case of the previously studied DNAs containing abasic sites, the placement of an abasic site within the dA tract gives rise to α and β forms which are different from each other and from the undamaged DNA up to four base pairs away from the damaged site.

MATERIALS AND METHODS

Sample Preparation. Single-strand DNAs of the sequences 5′-d($C_1G_2C_3A_4A_5A_6A_7A_8T_9G_{10}C_{11}G_{12}$)-3′ and 5′-d($C_1G_2C_3A_4T_5T_6U_7T_9G_{10}C_{11}G_{12}$)-3′ were obtained from DNAgency. The purity of the single strands was checked by reverse phase HPLC using a Hamilton PRP-1 column with an elution gradient of 0 to 12.5% acetonitrile in 25 mM phosphate buffer at pH 7.0. The single strands were dialyzed against H_2O, lyophilized, and then dissolved in buffer containing 10 mM sodium phosphate, 100 mM sodium chloride, and 0.05 mM EDTA at pH 7.0.

The single-strand 5′-d($C_1G_2C_3A_4T_5T_6D_7T_9T_8G_{10}C_{11}G_{12}$)-3′ containing an abasic site, D, at position 7 was prepared by enzymatic removal of uracil from 5′-d($C_1G_2C_3A_4T_5T_6$-$U_7T_8T_9G_{10}C_{11}G_{12}$)-3′ using *N*-uracil glycosylase and reaction conditions that have been previously described (*9*, *57*−*59*). The reaction was carried out in 40 mM HEPES buffer at pH 7.5 containing 70 mM NaCl and 2 mM EDTA with a 1:1 ratio of DNA:enzyme. The reaction was monitored using the reverse phase HPLC method described above which cleanly separates free uracil, the parent ssDNA containing dU, and the ssDNA reaction product which contains an abasic site. The retention time for the undamaged, parent ssDNA is 15 min, while that of the abasic ssDNA product is 20 min. The reaction was stopped when the HPLC peak corresponding to the parent DNA dropped below the sensitivity of the detector. The total time for enzymatic removal of U from this ssDNA was 10 days compared to about 1 h for the normal sequences we have used under the same reaction conditions (*9*, *57*−*59*). Sequence-dependent rate differences of about this magnitude for the uracil glycosylase reaction have been previously reported (*60*, *61*).

Abasic site-containing ssDNA was purified from the reaction mixture by gel chromatography using a preparative TSK-GEL G2000SW column and eluting with 25 mM sodium phosphate buffer at pH 7.0 buffer containing 100 mM sodium chloride. Purified abasic ssDNA was dialyzed against distilled H_2O, lyophilized, and then reconstituted in pH 7.0 buffer containing 10 mM sodium phosphate, 100 mM sodium chloride, and 0.05 mM EDTA in 99.96% ^2H_2O.

The heteroduplex for the NMR studies was formed from equimolar amounts of the two singled-stranded DNAs using

the extinction coefficients of each strand. The actual titration of the abasic strand with the dA tract ssDNA to form the duplex was monitored by one-dimensional proton NMR. The resulting duplex was then lyophilized several times from ^2H_2O to remove residual H_2O. Lyophilized duplex was then dissolved in 0.4 mL of pH 7.0 buffer containing 10 mM sodium phosphate, 100 mM sodium chloride, and 0.05 mM EDTA in 99.96% ^2H_2O at a final sample concentration of 2.5 mM duplex.

NMR Procedures. Two-dimensional NMR data were acquired at 400 MHz on a Varian Unityplus spectrometer at Wesleyan, at 500 MHz on a Varian Inova spectrometer at Wesleyan, and at 750 MHz on a Bruker DMX spectrometer at the University of Wisconsin (Madison, WI). The Varian NMR data were processed using VNMR software and the Bruker data using Felix 950 software.

NOESY[1] experiments were run on the Bruker 750 spectrometer with the sample in ^2H_2O at 20 °C with mixing times of 100 and 250 ms and a 2 s equilibration delay. The spectral width in each dimension was 11 095 Hz. Eight hundred t_1 increments were acquired with 16 transients per t_1 point and 2K complex points in the t_2 dimension. The data were processed with a sinebell apodization in both dimensions prior to 4K × 2K Fourier transformation. These data were used for NOESY cross-peak quantification. NOESY data on the sample in normal water were obtained at a mixing time of 150 ms, and a Watergate pulse train was used for suppression of the water signal. Additional 500 MHz NOESY experiments were run with the sample in normal water using a mixing time of 200 ms with the sample at 20 °C.

All data collected on the Varian 400 MHz instrument were found using a sample temperature of 25 °C with the exception of a 250 ms NOESY experiment which was run at 20 °C. NOESY data were collected at 400 MHz in ^2H_2O with mixing times of 100, 250, and 300 ms. NOESY experiments were collected with a spectral width of 4000 Hz in both dimensions with 128 transients collected for each of the 600 t_1 increments. Sinebell apodization was applied prior to 2K × 1K Fourier transformation of the data.

A PECOSY spectrum was acquired at 400 MHz with ^{31}P decoupling during the evolution period. The data were collected as 2K complex points in t_2 and 512 complex points in t_1. The F_2 spectral width was 3200 Hz, and the F_1 spectral width was 2600 Hz. Two hundred fifty-six transients were acquired for each t_1 increment. A Gaussian weighting function was used in both dimensions, and the spectrum was zero-filled to 2K × 2K real points.

A TOCSY experiment with a mixing time of 60 ms was collected with the sample in ^2H_2O at 400 MHz. The residual water signal was presaturated during the 1.5 s equilibrium delay. The spectral width in both dimensions was 4000 Hz. Two thousand forty-eight complex points were collected in the t_2 dimension and 512 complex points in t_1. Gaussian weighting was applied prior to Fourier transformation, resulting in a spectrum of 2K × 1K real points.

A series of one-dimensional experiments were run to allow identification of the AH2 resonances on the basis of their relatively long T_1 values. These spectra were acquired with the sample in ^2H_2O at 400 MHz with a spectral width of 6000 Hz and 32 transients. An equilibrium delay of 5 s was used, and the T_1 delay time was arrayed from 0.6 to 1.17 s in 0.03 s steps.

A 500 MHz, 125 ms ROESY experiment in ^2H_2O was performed at 25 °C. A spectral width of 6000 Hz was used in each dimension. The data were collected as 2K complex t_1 points and 512 complex t_2 points. Gaussian weighting was applied in both dimensions, and the data were zero-filled to yield a spectrum of 2K × 2K real points.

Quantitation of NOE Cross-Peak Volumes. NOE cross-peak volumes were quantified in the data obtained at 750 MHz with mixing times of 100 and 250 ms using FELIX 950 software as previously described (*56*, *57*, *62*).

Structure Determination Procedures. Structure refinement by restrained molecular dynamics using X-PLOR 3.1 was performed as previously described with the following modifications (*56*, *57*, *62*). The optimum weighting of the NOE constraints and dihedral constraints was found to be 60 kcal/mol. For each mixing time, 352 NOE volume constraints were used for the α structure and 353 for the β structure and the refinements of the two structures were carried out independently. Forty-eight dihedral constraints (H1′-C1′-C2′-H2′ and H1′-C1′-C2′-H2″) were used for both the α and β structures. The nonbonded interaction cutoff was set to 11.5 Å. The distance over which the nonbonded interaction was switched from on to off was 9.5−10.5 Å. The distance cutoff for the Watson−Crick hydrogen bonding interactions was set to 7.5 Å, and the switching function was applied from 5.5 to 6.5 Å.

Starting structures were generated from canonical B-DNA by replacing the base with a hydroxyl group at the C1′ α or β position of the abasic site. The α and β structures were refined separately. Starting structures were energy minimized by 100 steps of Powell's conjugate gradient minimization using X-PLOR. The restraints based on the experimental results are sufficiently large that the same structures are obtained when starting from A- or B-DNA. The rmsd of the final β structure relative to the minimized structure at the beginning of the trajectory was 3.1 Å and 2.4 Å for the α.

Relaxation matrix refinements were carried out at 300 K in a vacuum. Starting, minimized structures were subjected to 100 steps of minimization using the force field with all restraints. This was followed by a 100 ps relaxation matrix simulation and 200 steps of conjugate gradient minimization. Each trajectory was run for 100 ps, and the structures appeared to reach equilibrium after 50 ps. The structures from 70 to 80 ps were each used to generate a back-calculated spectrum, and these back-calculated spectra were then averaged for comparison with the experimental results.

The NOE cross-peak volumes for each of these structures were back-calculated separately using an overall correlation time of 5 ns, a leakage rate of 0.33 s^{-1}, and a distance cutoff of 5.5 Å. Back-calculated cross-peak volumes for each 2 ps time point were averaged for a 10 ps time frame to create a predicted spectrum. The NMR *R*, *Q*, and rms (*63*) values for the fit of the predicted and experimental NOEs for the α structure at 76 ps are 0.81, 0.44 and 0.64, respectively, while the values for the average over 70−80 ps are 0.78, 0.44,

[1] Abbreviations: NOESY, nuclear Overhauser effect spectroscopy; NOE, nuclear Overhauser effect; TOCSY, total correlation spectroscopy; DQCOSY, double-quantum filter correlation spectroscopy; ECOSY, easy correlation spectroscopy; PECOSY, phased easy correlation spectroscopy; heterotocsy, heteronuclear total correlation spectroscopy.

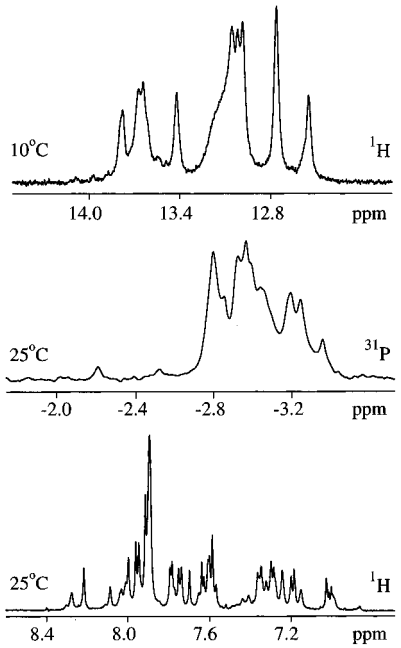

FIGURE 1: The top spectrum is the 400 MHz imino proton region of 5′-d($C_1G_2C_3A_4A_5A_6A_7A_8T_9G_{10}C_{11}G_{12}$)-3′ paired with 5′-d($C_{13}G_{14}C_{15}A_{16}T_{17}T_{18}D_{19}T_{20}T_{21}G_{22}C_{23}G_{24}$)-3′, where D indicates the abasic site. The middle spectrum is the 161 MHz proton-decoupled phosphorus spectrum of the same DNA duplex. The bottom spectrum is the 400 MHz proton spectrum showing the aromatic protons.

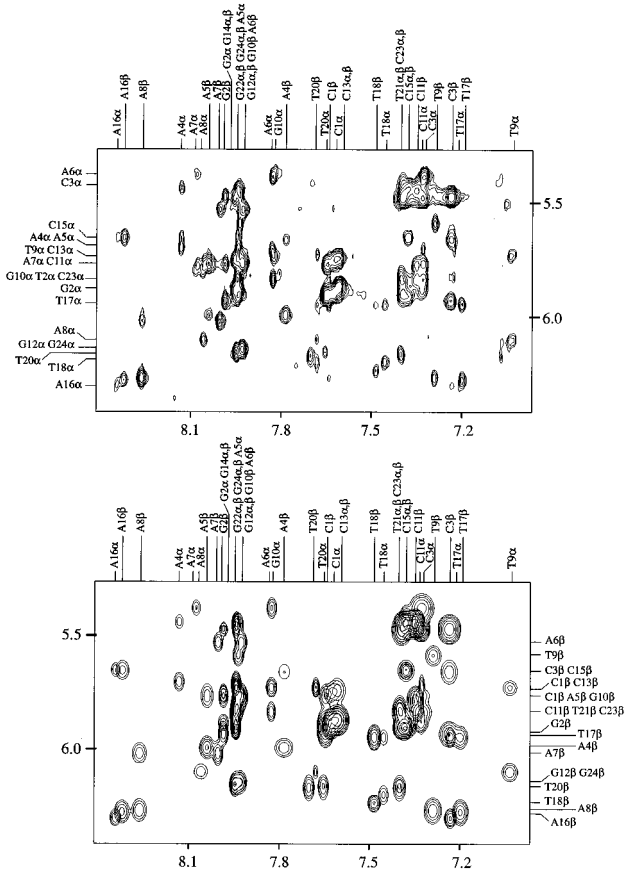

FIGURE 2: The top spectrum contains the aromatic to H5 and H1′ region of the two-dimensional 750 MHz NOESY spectrum obtained with a mixing time of 250 ms. The bottom spectrum shows the same region of the predicted NOESY spectrum. Indicated on the top axis are the assignments of all H8 and H6 aromatic protons for the sequence 5′-d($C_1G_2C_3A_4A_5A_6A_7A_8T_9G_{10}C_{11}G_{12}$)-3′ paired with 5′-d($C_{13}G_{14}C_{15}A_{16}T_{17}T_{18}D_{19}T_{20}T_{21}G_{22}C_{23}G_{24}$)-3′. Indicated on the experimental spectrum are the H5 and H1′ assignments for the α form and on the predicted spectrum the H5 and H1′ assignments for the β form.

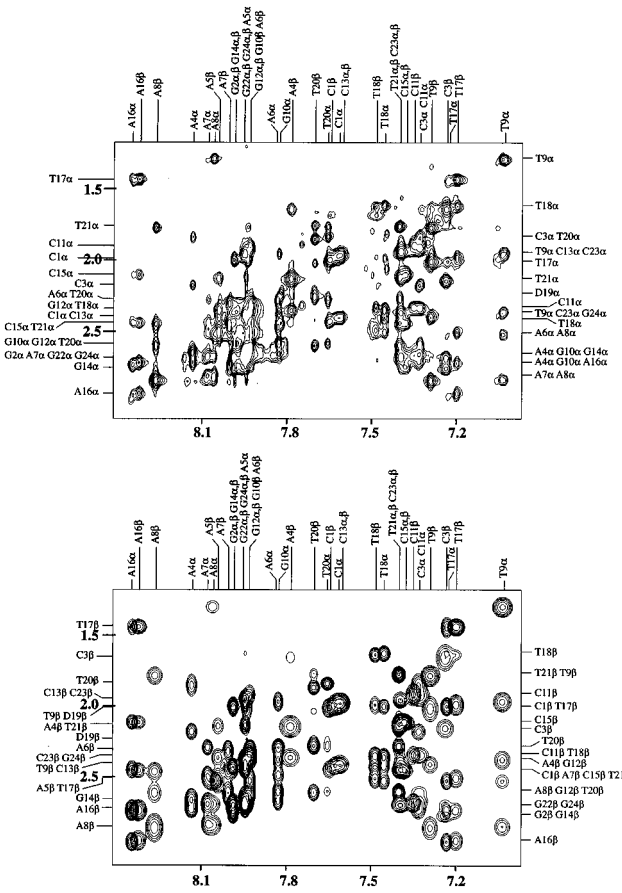

FIGURE 3: The top spectrum contains the aromatic and H2′ and H2″ region of the two-dimensional 750 MHz NOESY spectrum obtained with a mixing time of 250 ms. The bottom spectrum shows the same region of the predicted NOESY spectrum. Indicated on the top axis are the assignments of all H8 and H6 aromatic protons. Indicated on the experimental spectrum are the H2′, H2″, and methyl resonance assignments for the α form and on the predicted spectrum the H2′, H2″, and methyl resonance assignments for the β form.

and 0.64, respectively. The NMR *R*, *Q*, and rms for the β structure at 76 ps are 0.69, 0.41, and 0.70, respectively, while the values for the average over 70−80 ps are 0.66, 0.39, and 0.68, respectively. These values are somewhat higher than those we have obtained for other damaged duplex DNA (*47*, *57*, *62*). Averaging only lowers these statistical measures of the quality of the agreement between the predicted and experimental results. The all-atom rmsd between the α structures in the 70−80 ps time period is 2.59 Å and for the β structures 2.53 Å. This value for the rmsd over the 10 ps interval is consistent with a relatively high level of conformational mobility near the damaged site as discussed next. The restraint file for the α structure is R1SJKMR and the PDB structure file 1SJK, and the restraint file for the β structure is R1SJLMR and the PDB structure file 1SJL. These are available from the Brookhaven Protein Data Bank.

Averaging was found to be needed since no one structure was found to be consistent with all of the observed NOEs. The individual structures typically predicated almost all of the NOEs properly, as indicated by the *R*, *Q*, and rms values. However, there were typically a few NOEs which were much better predicted by averaging. For example, a cross-peak between αT_{20} H1′ and αT_{21} H6 is absent in the spectrum generated from the 80 ps structure yet present at 70, 72, 74,

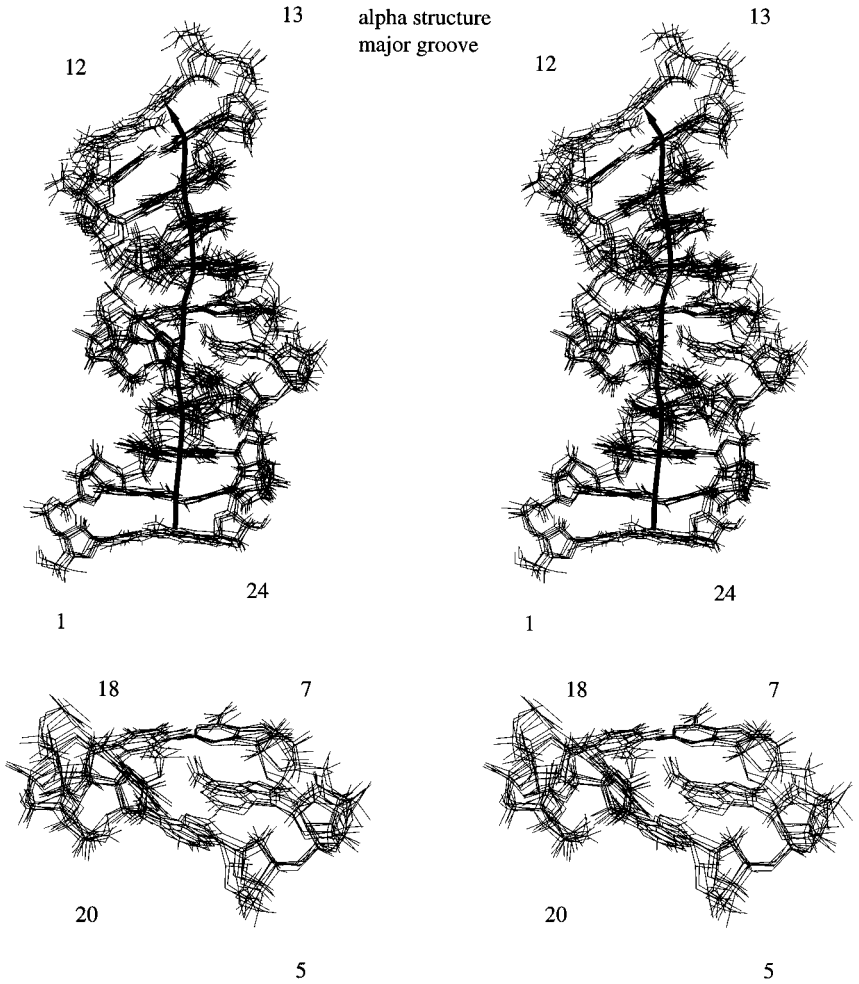

FIGURE 4: Stereoview of the α form of the DNA duplex containing an abasic site. Overlaid are the structures obtained every 2 ps in the 70−80 ps interval of the dynamics trajectory. The structures are shown with the major groove being prominent. The helical axis at each time point is also shown. At the bottom is an expanded view of the central three base pairs, including the abasic site and adjacent base pairs.

76, and 78 ps with intensities of 82, 63, 109, 76, and 5, respectively, in arbitrary volume units. The average of the αT_{20} H1′−αT_{21} H6 back-calculated cross-peak intensities from 70 to 80 ps is 63, in agreement with the experimental cross-peak intensity of 64. Similarly, a back-calculated cross-peak between αT_{20} H6 and αD_{19} H3′ is absent at 70 and 80 ps, yet at 72, 74, 76, and 78 ps, this cross-peak has an intensity of 14, 18, 32, and 13, respectively, in arbitrary volume units. The 70−80 ps average of the predicted αT_{20} H6−αD_{19} H3′ cross-peak intensity is 13 compared to 20 for the experimental peak. Averaging allows each cross-peak to be represented in the predicted spectrum in agreement with the experimental data. The cross-peak between αA_{16} H8 and the αT_{17} methyl proton, although present in all back-calculated spectra, has intensities of 157, 142, 242, 176, 234, and 117 at 70, 72, 74, 76, 78, and 80 ps, respectively, in arbitrary volume units. Averaging of these cross-peak intensities gives a value of 178 which more closely agrees with the experimental value of 180 than most of the individual time points. Averaging over 10 ps was found to be sufficient to obtain agreement between experimental and predicted spectra. We are now examining the possibility of developing of statistical measures which will more precisely reflect the quality of agreement of the experimental and predicted results than is obtained with the *R*, *Q*, and rms values as well as refining the structure with water molecules present.

The accessible surfaces were calculated using the Connolly surface calculation in Insight II essentially as described previously (*62*). Probe radii were incremented in 0.2 Å steps between 0.2 and 4.0 Å. The accessible surfaces were calculated separately for the bases of A_4, A_5, A_6, A_7, A_8, T_{17}, T_{18}, T_{20}, and T_{21} in both the α and β structures. These surface areas were normalized to the accessible surface of a free A or T base using the same probe radii before plotting. The accessible surfaces of the D_{19} sugar in both the α and β forms were normalized to that of a free deoxyribose.

RESULTS AND DISCUSSION

Some of the basic properties of the damaged, abasic site-containing DNAs can be ascertained from the one-dimensional spectra shown in Figure 1. The spectrum of the nonexchanging protons with resonances in the aromatic region indicates that two, or more, forms of DNA are present as there are more signals in this region than can be accounted for by the presence of a single structure. The resonances in the aromatic region are sharp, and this indicates that the structures are stable and that intermediate rate exchange between the structures does not occur on the NMR time scale.

The imino region of the spectrum can contain information about the number of base pairs present, and the net integrated intensity in this region is consistent with all of the possible base pairs being present. This indicates, in particular, that

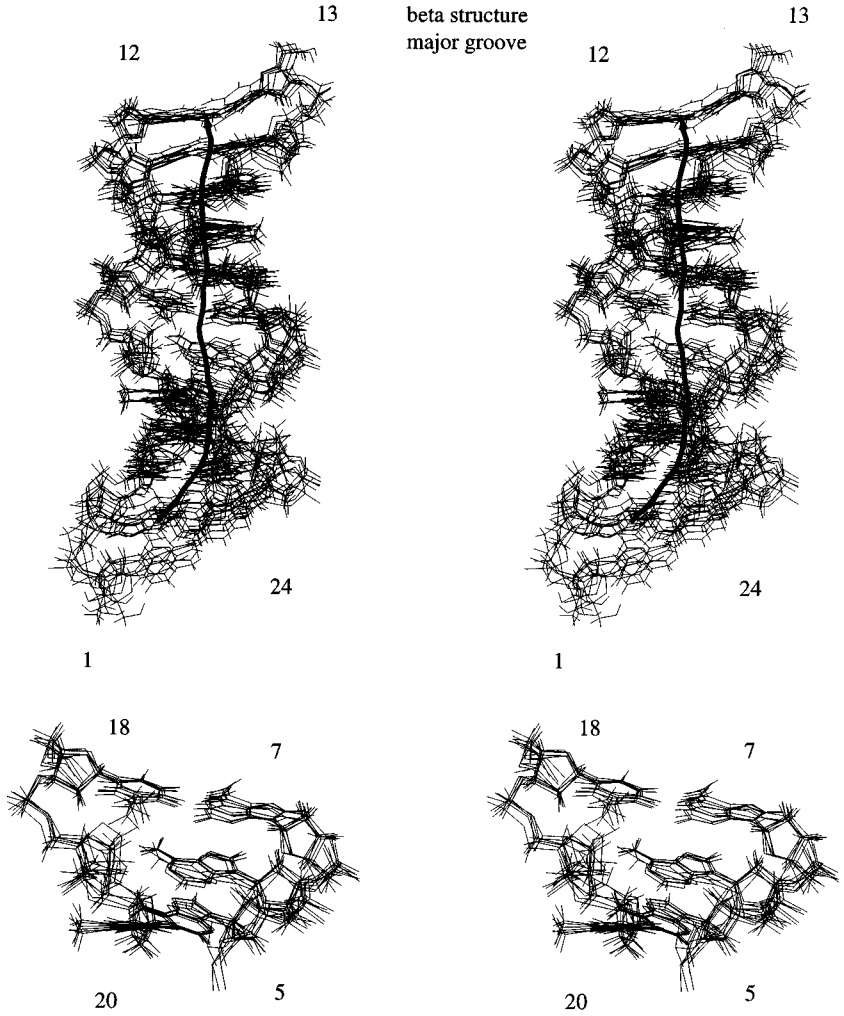

FIGURE 5: Stereoview of the β form of the DNA duplex containing an abasic site. Overlaid are the structures obtained every 2 ps in the 70−80 ps interval of the dynamics trajectory. The structures are shown with the major groove being prominent. The helical axis at each time point is also shown. At the bottom is an expanded view of the central three base pairs, including the abasic site and adjacent base pairs.

the two A-T base pairs adjacent to the abasic site are present. The examination of the imino proton−AH2 NOEs indicated that there is extensive overlap of the resonances of the imino protons of the α and β forms.

The phosphorus spectrum shows that most of the signals are in the region typically associated with B-DNA. The phosphorus spectrum was not assigned as it is typically difficult to relate these chemical shifts to structural features. Taken together, these one-dimensional results indicate that the α and β forms of the damaged DNAs adopt stable structures which can be studied in detail.

The helix opening and closing rates of this damaged DNA have not been determined. The determination of the helix opening and closing times requires observing the exchange rates of the imino protons as a function of the concentration of a base catalyst. Unfortunately, the base will also induce the β-elimination of the abasic site. In an earlier study, the helix opening and closing rates of a normal duplex DNA containing an abasic site were obtained, but this study required the sacrifice of many DNA samples (*58*).

A wide range of two-dimensional proton NMR data were obtained on the sample. The assignment of the proton resonances of this DNA was relatively challenging due to the extensive differences between the α and β forms. In the abasic site-containing DNAs, we have previously examined the structural effects of the damaged site only extended to the nearest neighbor base pairs of the damaged site. At all other positions, the α and β forms were found to be much the same. In the case where the abasic site is in the middle of the dA tract region, the differences between the α and β forms extended essentially throughout the DNA. Thus, the α and β forms differ from each other as well as the parent DNA more or less throughout. For example, the chemical shift of the H6 of T_9 is about 0.3 ppm more upfield in the α form than in the β form and T_9 is four residues away from the damaged site and is on the strand complementary to the one containing the damaged site. The resolution possible with 750 MHz data helped make the assignments possible.

The results of NOESY experiments at several mixing times along with TOCSY and ROESY data allowed identification of the sequential connectivities that were used to make the assignments. Many of the assignments are indicated in Figures 2 and 3. Once the cross-peaks were assigned, the NOE volumes were used as restraints to determine the structures of the α and β forms of the DNA independently as described above. The structures were used to back-calculate the NOESY spectra, and the predicted and experimental spectra are shown in Figures 2 and 3 for comparison purposes.

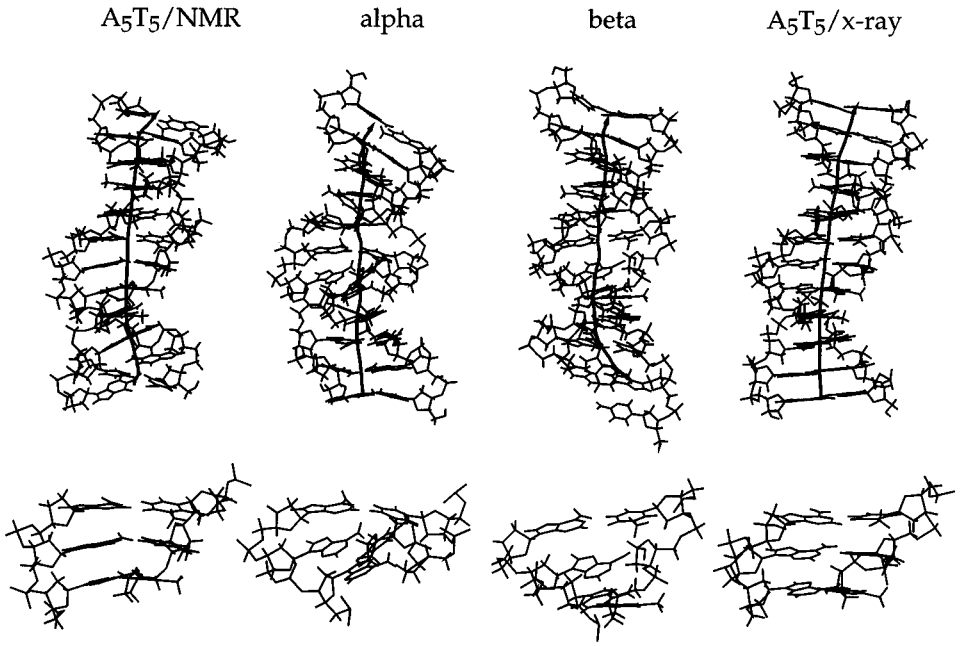

FIGURE 6: α and *β* structures of the damaged, abasic DNA duplex with the undamaged parent DNA structures as determined by NMR and X-ray crystallography are shown with the minor groove being prominent. The α and *β* structures were obtained at the 76 ps point of the trajectory. The X-ray structure is that of the up form. The central three base pairs of each structure, including the abasic site and adjacent base pairs, are expanded at the bottom. The helical axes are also indicated.

The predicted spectra represent an average over 10 ps of the trajectory. The structures obtained from 70 to 80 ps in the trajectory were taken at 2 ps intervals, and each was used to back calculate the spectrum. The predicted spectrum is the simple average of this set of spectra. To help illustrate the extent of the structural fluctuation that occurs over this interval of the trajectory, Figure 4 contains the overlay of the α structures and Figure 5 the overlay of the *β* structures obtained at 2 ps time intervals from 70 to 80 ps. The overlays show that there is not much difference between the structures over this time range, except for the terminal base pairs which have fewer experimental restraints than the internal base pairs. An average was found to be needed since no one structure was found to be consistent with all of the NOEs as discussed above.

The 10 ps time scale of a trajectory does not necessarily correspond to 10 ps of real time due to the presence of the restraints based on the experimental information. The range of structures shown is indicative of the range of structures consistent with the experimental data rather than the range of structures these molecules adopt over a 10 ps time period. The line width and ROESY data indicated that no exchange between structures occurs on the time scale of a few to a few hundreds of milliseconds. Interconversion between the α and *β* forms occurs through the hydrated aldehyde, as discussed above, and is typically on the time scale of seconds (*13*).

The structures of the α and *β* forms are quite different from each other, and the differences are not limited to the damaged site and the base pairs immediately adjacent to the damaged site. The depictions of the structures shown indicate that the *β* form is mostly closer to B-DNA than the α form. The *β* structure has a fairly straight helical axis except at the ends which are not as well-defined as the internal regions. The 12-13 terminal base pair exhibits more motion in the trajectory of the *β* structure over this time range. The strand containing the damaged site in the α form adopts a somewhat compressed structure near the damaged site as shown.

The structures of the two damaged forms of this DNA are shown along with the structures of the undamaged DNA as determined by NMR and X-ray methods in Figures 6 and 7. The minor groove of the DNAs is prominent in the structures shown in Figure 6. In this view, the almost uniform spacing of the dA residues through the dA tract observed in the undamaged DNA is lost in the damaged DNAs. The curvature of the undamaged DNAs resulting from the dA tracts is also apparently lost due to the presence of the damaged site. The α and *β* damaged sites appear to be lacking the structural continuity that gives rise to the bending in the parent, undamaged DNA. The stacking of the dA residues is more pronounced in the *β* structure than in the α structure with the *β* structure having dA stacking relatively similar to that of the undamaged DNA.

Structures of duplex DNAs containing tetrahydrofuran analogues of the naturally occurring abasic site have been determined (*64*−*68*). These studies have indicated that duplex DNAs with the analogue of the abasic site form a single structure consistent with the analogue having a single form. The structures of these DNAs are all B form, right-handed structures with the structure of the DNA being perturbed essentially only at and directly adjacent to the altered site. When adenosine is the base opposite the tetrahydrofuran, then the adenosine is stacked in the helix. When a thymine was placed opposite the tetrahydrofuran site, the thymine was also stacked. These structures have been compared to those of DNAs containing single-base bulges (*68*).

The structures of normal DNAs containing naturally occurring abasic sites (*9*, *57*−*59*) are generally similar to

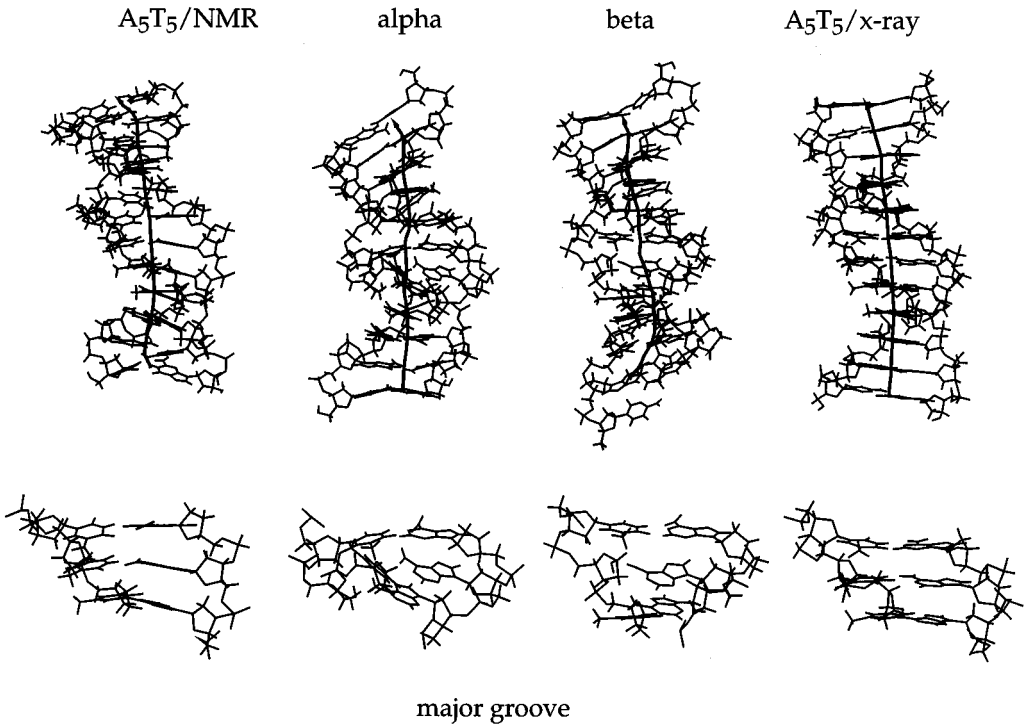

FIGURE 7: The α and β structures of the damaged, abasic DNA duplex with the undamaged parent DNA structures as determined by NMR and X-ray crystallography are shown with the major groove being prominent. The α and β structures are those at the 76 ps point of the trajectories. The X-ray structure is that of the up form. The central three base pairs of each structure, including the abasic site and adjacent base pairs; are expanded at the bottom. The helical axes are also indicated.

those obtained on the DNAs containing tetrahydrofuran sites. The structures differ from those of the analogous undamaged DNAs except at and directly adjacent to the site of damage. When adenosine is opposite the abasic site, the adenosine is stacked. Other residues may not be completely stacked, though detailed structures of DNAs with residues other than adenosine opposite an aldehydic abasic site have not yet been published. The structures of the duplexes containing the α and β forms have been found to be different, but these differences are limited to the damaged site and the immediately adjacent base pairs.

The results presented here are quite different from those previously obtained on both the tetrahydrofuran analogue and the naturally occurring abasic sites. The presence of an abasic site in the dA tract disrupts the structure relative to the parent DNA up to four base pairs away from the site of damage. The structures of the α and β forms are different up to four base pairs away from the site of damage. This shows that the hemiacetal form of the abasic site can be a strong determinant of the structure of the DNA, and this type of information cannot be obtained from the tetrahydrofuran analogues.

The solvent accessible surfaces of the residues at the damaged site and of the residues in the two adjacent base pairs were examined. In a prior study on a damaged DNA containing a thymine glycol residue, the percent of the surface area of a residue that is accessible to a probe molecule with a radius of about 2−4 Å was shown to be a way to quantify the "extrahelicity" or accessibility of residues (*62*). Similar calculations were performed on these DNAs with the percent accessible surfaces shown as a function of probe radius in Figure 8. A normal, internal residue in B-DNA has a percent accessible surface area of less than 20% to a probe of radius 2−4 Å (*62*). The accessibility of the abasic site may be a prime determinant for the ability of enzymes

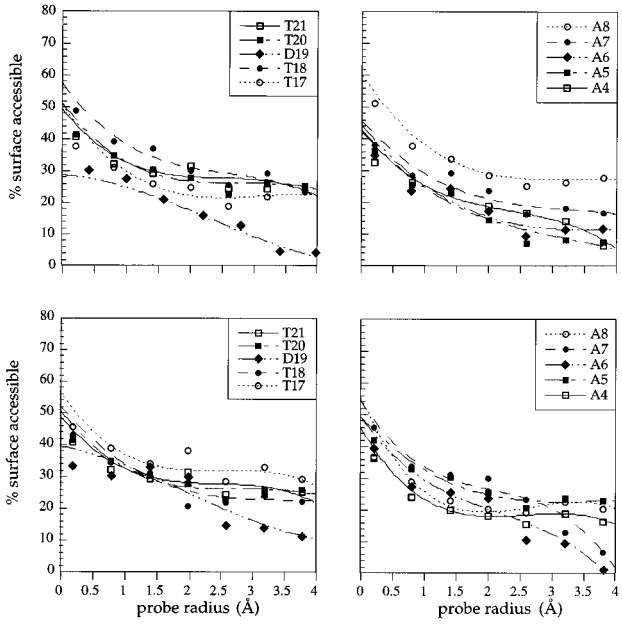

FIGURE 8: The top graphs represent the accessibile surface of the abasic site and two adjacent base pairs for the α form of the DNA duplex. The bottom graphs show the surface accessibilities of the same residues of the β form. The accessibilities of the abasic site-containing strand are on the left. Accessibilities of the dA residues on the strand opposite the abasic strand are graphed on the right.

such as those of the helix−hairpin−helix motif to detect its presence (*69*).

The plots show that for the strand containing the abasic site in the α structure there is a moderately high accessibility up to two base pairs away from the damaged site. On the opposing strand, A_8 which is two residues away from the damaged site has extra accessibility whereas some of the residues closer to the damaged site have more normal

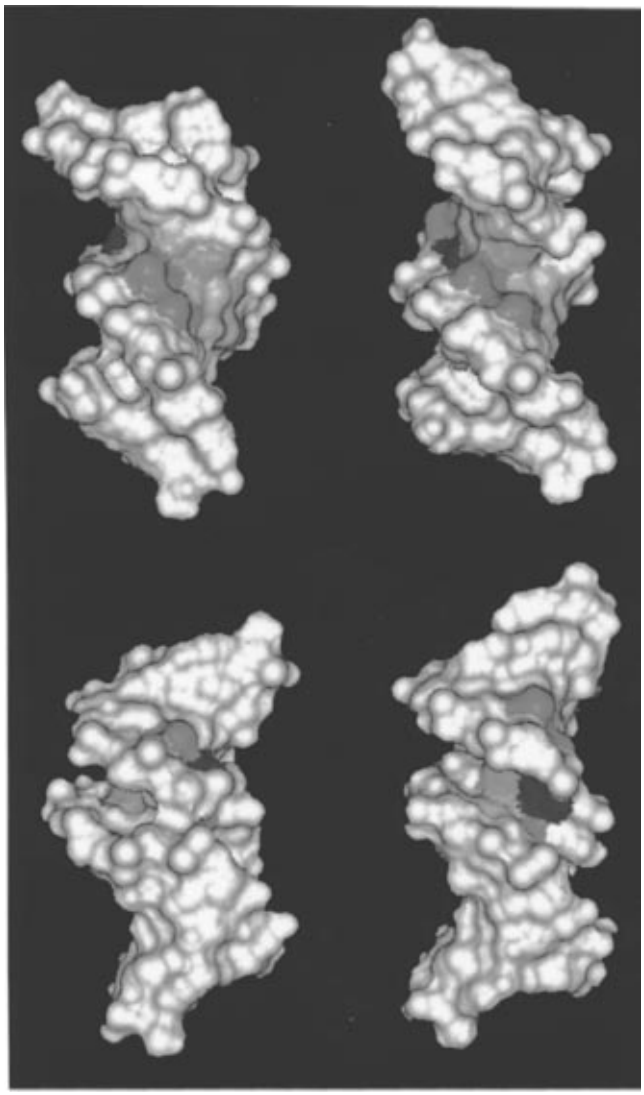

FIGURE 9: The accessible surfaces of the α (left) and β (right) forms of the DNA duplex are viewed from the major groove (top) and the minor groove (bottom). The accessible surface is that calculated with a probe radius of 1.4 Å. The abasic deoxyribose hemiacetals are shown in blue, and the base of A_6, opposite the abasic site, is in red. The bases of A_4, A_5, A_7, and A_8 are shown in orange, and those of T_{17}, T_{18}, T_{20}, and T_{21} are shown in green.

accessibilities. The plots show that for the strand containing the abasic site in the β structure there is increased accessibility up to two base pairs away from the damaged site and in particular for T_{17}. On the opposing strand, there is relatively little extra accessibility with none of the residues being over 30% accessible at 4 Å.

The accessible surfaces of the DNAs are shown in Figure 9. The surfaces show that the residues near the damaged site have about the same accessibility from the major grooves in both the α and β forms. The view from the minor groove shows that the β form has both the abasic site and the opposing dA residue considerably more accessible than is the case for the α form. This figure also shows that from the perspective of the van der Waals surfaces the two forms of the damaged DNA are more similar than from the perspective of the stick structures. The accessible surfaces look much the same for all of the structures in the 70−80 ps region of the trajectory.

These results indicate that the presence of a damaged site may have pronounced effects that occur distant to the location of the damaged site. The presence of an abasic site in a dA tract leads to a significant change in the stable curvature found in the absence of the damaged site. The elimination of the curvature can lead to changes in the interactions between regions that are distant from one another in sequence or with proteins that are bound to regions brought together by the stable curvature of DNA induced by dA tracts.

These results also indicate that the effects of DNA damage can be sequence-dependent in at least two ways. First, the structures of the abasic site-containing damaged DNAs in a dA context are different from those of DNA containing an abasic site in more normal sequence context. Second, the structures of the damaged DNA in the dA tract sequence context are more different from the parent, undamaged DNA than is observed for the damaged DNA in the more normal sequence context. Thus, the structure of damaged DNA is sequence context-dependent as is the structure of undamaged DNA. It appears that dA tracts have distinct properties in both the undamaged and abasic site cases. Additional studies on damaged DNA structures in different sequence contexts are underway.

ACKNOWLEDGMENT

The authors thank Dr. R. D. Beger for aiding in the preparation of the final version of the manuscript. The 750 MHz spectra were obtained with the assistance of Dr. Frits Abildgaard at the National Magnetic Resonance Facility at Madison (operation subsidized by the NIH Biomedical Research Technology Program under Grant RR02301; equipment funded by the University of Wisconsin NSF Academic Infrastructure Program under Grant BIR-9214394, the NIH Shared Instrumentation Program under Grants RR02781 and RR08438, the NIH Biomedical Research Technology Program under NIH Grant RR02301, the NSF Biological Instrumentation Program under Grant DMB-8415048, and the U.S. Department of Agriculture).

REFERENCES

1. Cadet, J. (1994) DNA damage caused by oxidation, deamination, ultraviolet radiation and photoexcited psoralens, *IARC Sci. Publ. 125*, 245−276.
2. Demple, B., and Harrison, L. (1994) Repair of oxidative damage to DNA: Enzymology and biology, *Annu. Rev. Biochem. 63*, 915−948.
3. Barnes, D. E., Lindahl, T., and Sedgwick, B. (1993) DNA repair, *Curr. Opin. Cell Biol. 5*, 424−433.
4. Freidberg, E. C. (1985) *DNA Repair*, Freeman, New York.
5. Holmes, G. E., Bernstein, C., and Bernstein, H. (1992) Oxidative and other DNA damages as the basis of aging: A review, *Mutat. Res. 275*, 305−315.
6. Lindahl, T. (1994) Instability and decay of the primary structure of DNA, *Nature 362*, 709−715.
7. Sonntag, C. V. (1987) *The chemical basis for radiation biology*, Taylor-Francis, London.
8. Ward, J. F. (1991) DNA damage and repair, in *Physical and chemical mechanisms in molecular radiation biology*, (Glass, W. A., and Varma, M. N., Eds.) p. 403−421, Plenum Press, New York.
9. Manoharan, M., Ransom, S. C., Mazumder, A., Gerlt, J. A., Wilde, J. A., Withka, J. M., and Bolton, P. H. (1988) Enzymatic synthesis of abasic sites in DNA heteroduplexes and their characterization by site specific labeling with ^{13}C, *J. Am. Chem. Soc. 110*, 1620−1622.
10. Manoharan, M., Mazumder, A., Ransom, S. C., Gerlt, J. A., and Bolton, P. H. (1988) Mechanism of UV endonuclease V cleavage of abasic sites in DNA determined by ^{13}C labeling, *J. Am. Chem. Soc. 110*, 2690−2692.

11. Mazumder, A., Gerlt, J. A., Rabow, L., Stubbe, J., and Bolton, P. H. (1989) UV Endonuclease V from bacteriophage T4 catalyzes DNA strand cleavage at aldehydic abasic sites by a syn β-elimination reaction, *J. Am. Chem. Soc. 111*, 8209−8210.
12. Mazumder, A., Gerlt, J. A., Absalon, M. J., Stubbe, J., Cunningham, R. P., Withka, J. M., and Bolton, P. H. (1991) Stereochemical studies of the β-elimination reactions at aldehydic abasic sites in DNA: Endonuclease III from *Escherichia coli*, sodium hydroxide and Lys-Trp-Lys, *Biochemistry 30*, 1191−1196.
13. Wilde, J. A., Bolton, P. H., Manoharan, M., Ransom, S. C., and Gerlt, J. A. (1989) Characterization of the equilibrating forms of the aldehydic abasic sites in duplex DNA by ^{17}O NMR, *J. Am. Chem. Soc. 111*, 1894−1895.
14. Bhagwat, M., and Gerlt, J. A. (1996) 3′ and 5′ strand cleavage reactions catalyzed by the Fpg protein from *Eschericha coli* occur via successive β- and δ-elimination mechanisms, respectively, *Biochemistry 35*, 659−665.
15. Lindahl, T. (1982) DNA repair enzymes, *Annu. Rev. Biochem. 51*, 61−87.
16. Loeb, L. A., and Preston, D. B. (1987) Mutagenesis by apurinic/apyrimidinic sites, *Annu. Rev. Genet. 20*, 201−230.
17. Frederico, L. A., Kunkel, T. A., and Shaw, B. R. (1990) Sensitive genetic assay for the detection of cytosine deamination. Determination of rate constants and the activation energy, *Biochemistry 29*, 2532−2537.
18. Frederico, L. A., Kunkel, T. A., and Shaw, B. A. (1993) Cytosine deamination in mismatched base pairs, *Biochemistry 32*, 6523−6530.
19. Mosbaugh, D. W., and Bennett, S. E. (1994) Uracil-excision DNA repair, *Prog. Nucleic Acid Res. 48*, 316−343.
20. Cathcart, R., Schniers, E., Saul, R. L., and Ames, B. N. (1984) Thymine glycol and thymidine glycol in human and rat urine: A possible assay for oxidative DNA damage, *Proc. Natl. Acad. Sci. U.S.A. 81*, 5633−5637.
21. Zhou, W., and Doetsch, P. W. (1993) Effects of abasic sites and DNA single-strand breaks on prokaryotic RNA polymerases, *Proc. Natl. Acad. Sci. U.S.A. 90*, 6601−6605.
22. Goodman, M. F., Creighton, S., Bloom, L. B., and Petruska, J. (1993) Biochemical basis of DNA replication fidelity, *Crit. Rev. Biochem. Mol. Biol. 28*, 83−126.
23. Driggers, W. J., LeDoux, S. P., and Wilson, G. L. (1993) Repair of oxidative damage within the mitochondiral DNA of RINr38 cells, *J. Biol. Chem. 268*, 22042−22045.
24. Leadon, S., and Lawrence, D. A. (1992) Strand-selective repair of DNA damage in the yeast GAL 7 gene required RNA polymerase II, *J. Biol. Chem. 267*, 23175−23182.
25. Weeda, G., and Hoeijmakers, J. H. J. (1993) Genes controlling nucleotide excision repair in eukaryotic cells, *BioEssays 15*, 249−258.
26. Selby, C. P., and Sancar, A. (1993) Molecular mechanism of transcription-repair coupling, *Science 260*, 53−58.
27. Chen, R.-H., Maher, V. M., Brouwer, J., Putte, J. v. d., and McCormick, J. J. (1992) Preferential repair and strand-specific repair of benzo-A-pyrene diol epoxide adducts in the HPRT gene of diploid human fibroblasts, *Proc. Natl. Acad. Sci. U.S.A. 89*, 5413−5417.
28. Elledge, S. J. (1996) Cell cycle checkpoints: Preventing an identity crisis, *Science 274*, 1664−1672.
29. Nasmyth, K. (1996) Viewpoint: Putting the cell cycle in order, *Science 274*, 1643−1645.
30. Sherr, C. J. (1996) Cancer cell cycles, *Science 274*, 1672−1677.
31. Stillman, B. (1996) Cell cycle control of DNA replication, *Science 274*, 1659−1664.
32. Hollander, M. C., Zhan, Q., Bae, I., and Fornace, A. J. (1997) Mamallian GADD34 an apoptosis and DNA damage-inducible gene, *J. Biol. Chem. 272*, 13731−13737.
33. Leadon, S. A., and Cooper, P. K. (1993) Preferential repair of ionizing radiation-induced damage in the transcribed strand of an active human gene is defective in Cockayne syndrome, *Proc. Natl. Acad. Sci. U.S.A. 90*, 10499−10503.
34. Klupp, B. G., Baumeister, J., Karger, A., Visser, N., and Mettenleiter, T. C. (1994) Identification and characterization of a novel structural glycoprotein in pseudorabies virus, gL, *J. Virol. 68*, 3868−3878.
35. Stuart, D. T., Upton, D. C., Higman, M. A., Niles, E. G., and McFadden, G. (1993) A poxvirus-encoded uracil DNA glycosylase is essential for virus viability, *J. Virol. 67*, 2503−2512.
36. Rao, K. S., and Loeb, L. A. (1992) DNA damage and repair in brain: relationship to aging, *Mutat. Res. 275*, 317−329.
37. Millins, A. K., Carpenter, M. S., and DeLange, A. M. (1994) The vaccina virus-encoded uracil DNA glycosylase has an essential role in viral DNA replication, *Virology 198*, 504−513.
38. Chen, Y.-H., and Bogenhagen, D. F. (1993) Effects of DNA lesions on transcription elongation by T7 RNA polymerase, *J. Biol. Chem. 268*, 5849−5855.
39. Sanchez, G., and Mamet-Bradley, M. D. (1994) Transcription by T7 RNA polymerase of DNA containing abasic sites, *Environ. Mol. Mutagen. 23*, 32−36.
40. Cai, H., Bloom, L. B., Eritja, R., and Goodman, M. F. (1993) Kinetics of deoxyribonucleotide insertion and extension at abasic template lesions in different sequence contexts using HIV-1 reverse transcriptase, *J. Biol. Chem. 268*, 23567−23572.
41. Kingma, P. S., and Osheroff, N. (1997) Spontaneous DNA damage stimulate topoisomerase II-mediated DNA cleavage, *J. Biol. Chem. 272*, 7488−7493.
42. Maccabee, M., Evans, J. S., Glackin, M. P., Hatahet, S., and Wallace, S. S. (1994) Pyrimidine ring fragmentation products. Effects of lesion structure and sequence context on mutagenesis, *J. Mol. Biol. 236*, 514−530.
43. Shibutani, S., and Grollman, A. P. (1993) Molecular mechanism of transcription-repair coupling, *J. Biol. Chem. 268*, 11703−11710.
44. Sandell, L. L., and Zakian, V. (1993) Loss of a yeast telomere: Arrest, recovery, and chromosome loss, *Cell 75*, 729−739.
45. Harrington, R. E. (1992) DNA curving and bending in protein-DNA recognition, *Mol. Microbiol. 6*, 2549−2555.
46. Ohyama, T. (1996) Bent DNA in the human adenovirus type 2 E1A enhancer is an architechtural element for transcription stimulation, *J. Biol. Chem. 271*, 27823−27828.
47. Tsai, M.-M., Fu, Y.-H. F., and Deonier, R. C. (1990) Intrinsic bends and integration host factor binding at F plasmid oriT, *J. Bacteriol. 172*, 4603−4609.
48. Cobbett, C., Dickson, B., and Farmer, L. (1989) The role of a static bend in the DNA of the aroF regulatory region of *Escherichia coli*, *Gene 75*, 185−191.
49. Lavigne, M., Roux, P., Buc, H., and Schaeffer, F. (1997) DNA curvature controls termination of plus strand DNA synthesis at the centre of HIV-1 genome, *J. Mol. Biol. 266*, 507−524.
50. Price, M. A., and Tullius, T. D. (1993) How the structure of an adenine tract depends on sequence context: a new model for the structure of TnAn DNA sequences, *Biochemistry 32*, 127−136.
51. Harrington, R. E. (1993) Studies of DNA bending and flexibility using gel electrophoresis, *Electrophoresis 14*, 732−746.
52. Koo, H.-S., Wu, H.-M., and Crothers, D. M. (1986) DNA bending at adenine.thymine tracts, *Nature 320*, 501−506.
53. Nadeau, J. G., and Crothers, D. M. (1989) Structural basis for DNA bending, *Proc. Natl. Acad. Sci. U.S.A. 86*, 2622−2626.
54. DiGabriele, A. D., Sanderson, M. R., and Steitz, T. A. (1989) Crystal lattice packing is important in determing the bend of a DNA dodecamer containing an adenine tract, *Proc. Natl. Acad. Sci. U.S.A. 86*, 1816−1820.
55. DiGabriele, A., and Steitz, T. A. (1993) A DNA dodecamer containing an adenine tract crystallizes in a unique lattice and exhibits a new bend, *J. Mol. Biol. 231*, 1024−1039.
56. Young, M. A., Goljer, I., Kumar, S., Srinivasan, J., Beveridge, D. L., and Bolton, P. H. (1995) Structure determination and analysis of local bending in an A-tract DNA duplex: comparison of results from crystallography, nuclear magnetic resonance and molecular dynamics simulations on d(CGCAAAAATGCG), *Methods Enzymol. 261*, 121−144.

57. Goljer, I., Kumar, S., and Bolton, P. H. (1995) Refined solution structure of a DNA heteroduplex containing an aldehydic abasic site, *J. Biol. Chem. 270*, 22980−22987.
58. Goljer, I., Withka, J. M., Kao, J. Y., and Bolton, P. H. (1992) Effects of the presence of an aldehydic abasic site on the thermal stability and rate of helix opening and closing of duplex DNA, *Biochemistry 31*, 11614−11619.
59. Withka, J. M., Wilde, J. A., Bolton, P. H., Mazumder, A., and Gerlt, J. A. (1991) Characterization of conformational features of a DNA heteroduplex containing an aldehydic abasic site, *Biochemistry 30*, 9931−9936.
60. Devchand, P. R., McGhee, J. D., and Sande, J. H. v. d. (1993) Uracil-DNA glycosylase as a probe for protein-DNA interactions, *Nucleic Acids Res. 21*, 3437−3443.
61. Kumar, N. V., and Varshney, U. (1994) Inefficient excision of uracil from loop regions of DNA oligomers by E. coli uracil DNA glycosylase, *Nucleic Acids Res. 22*, 3737−3741.
62. Kung, H. C., and Bolton, P. H. (1997) Solution structure of a duplex DNA containing a thymine glycol, *J. Biol. Chem. 272*, 9227−9236.
63. Withka, J. M., Srinivasan, J., and Bolton, P. H. (1992) Problems with, and alternatives to the NMR R factor, *J. Magn. Reson. 98*, 611−616.
64. Kalnik, M. W., Chang, C. N., Grollman, A. P., and Patel, D. J. (1988) NMR studies of abasic sites in DNA duplexes: Deoxyadenosine stacks into the helix opposite the cyclic analogue of 2-deoxyribose, *Biochemistry 27*, 924−931.
65. Kalnik, M. W., Chang, C. N., Johnson, F., Grollman, A. P., and Patel, D. J. (1989) NMR studies of abasic sites in DNA duplexes: Deoxyadenosine stacks into the helix opposite acyclic lesions, *Biochemistry 28*, 3373−3383.
66. Cuniasse, P., Fazakerley, G. V., Guschlbauer, W., Kaplan, B. E., and Sowers, L. C. (1990) The abasic site as a challenge to DNA polymerase. A nuclear magnetic resonance study of G, C and T opposite a model abasic site, *J. Mol. Biol. 213*, 303−314.
67. Cuniasse, P., Sowers, L. C., Eritja, R., Kaplan, B., Goodman, M. F., Cognet, J. A., LeBret, M., Guschlbauer, W., and Fazakerley, G. V. (1987) An abasic site in DNA. Solution conformation determined by proton NMR and molecular mechanics calculations, *Nucleic Acids Res. 15*, 8003−8022.
68. Coppel, Y., Berthet, N., Coulombeau, C., Coulombeau, C., Garcia, J., and Lhomme, J. (1997) Solution conformation of an abasic DNA undecamer duplex d(CGCACXCACGC)·d(GCGTGTGTGCG): The unpaired thymine stacks inside the helix, *Biochemistry 36*, 4817−4830.
69. Mullen, G. P., and Wilson, S. H. (1997) DNA polymerase β in abasic site repair: A structurally conserved helix-hairpin-helix motif in lesion detection by base excision repair enzymes, *Biochemistry 36*, 4713−4717.

BI971464L